

## IMAGE-BASED BRDF MEASUREMENT

Shachaf Weil-Zattelman and Fadi Kizel\*

Dept. of Mapping and Geoinformation Engineering, Technion - Israel Institute of Technology, Haifa, 32000, Israel  
[shaweil@campus.technion.ac.il](mailto:shaweil@campus.technion.ac.il); [fadikizel@technion.ac.il](mailto:fadikizel@technion.ac.il)

**KEY WORDS:** Remote sensing, Semi-empirical models, BRDF, SFM, Hyperspectral imaging, Graph theory.

### ABSTRACT:

One of the most challenging effects of remote sensing is landcover materials' Bidirectional Reflectance Distribution Function (BRDF). A wide range of approaches and measuring methods address the BRDF in various studies. However, there is a requirement for an accurate measurement setup and costly special equipment. Furthermore, the measurements and calculations are applied to model the BRDF for a single point on the object's surface. Considering these limitations, we propose a new modular framework and methodology for measuring, modeling, and analyzing the BRDF without the need for unique instruments. Instead, we suggest acquiring multiple overlapping images in a simple and time-saving way, sampling the desired object's Region Of Interest (ROI) in one image and automatically tracking it in the other images. Experimental results using laboratory data acquired under controlled conditions clearly show the advantages of our framework in retrieving the camera positions, tracking ROIs in the different images, and accurately measuring the BRDF of various land-cover types. Moreover, we observed the variability of the obtained measurements before and after applying the kernel-driven approach to minimize the BRDF effect. The results show that the applied correction reduces this variability significantly, indicating the high accuracy of measuring the directional reflectance using the proposed approach.

### 1. INTRODUCTION

A primary objective of remote sensing is to extract information about surfaces without direct contact. In this regard, spectral imaging is crucial for understanding surface characteristics, phenomena, and changes that occur to them (Shen et al., 2019). Nonetheless, extracting valuable information from spectral measurements is tricky due to several effects that incorporate undesired variability within the acquired data. One of these challenging effects is the Bidirectional Reflectance Distribution Function (BRDF) (Nicodemus et al., 1977). In the literature, it is customary to use a theoretical concept that describes radiation from a point source measured by a point sensor. However, such assumptions are not realistic in real applications. Thus, we refer to the BRDF term in this study, but we measure the Biconical Reflectance Factor (BCRF) in practice. The BCRF helps estimate the BRDF and is commonly used in remote sensing applications (Schaeppman-strub et al., 2006).

The BRDF causes the acquired spectral information of material to vary between acquisitions, thereby causing an undesired variability (Román et al., 2011). In addition, this variability also exists between the different pixels within the same scene. The BRDF effect has been addressed extensively. However, despite a large number of such research works, executing BRDF measurements is still a challenging task, and there are two main limitations in the existing approaches:

- 1) The measurement of the BRDF mainly relies on a unique instrument, e.g., a goniometer (Foo, 1997) (Riviere et al., 2012), which is usually expensive and not available in many labs.
- 2) The measurements are applied to model the BRDF of a single point or small area within the spectroradiometer field of view.

Considering these limitations, we propose a new framework for measuring and understanding the BRDF effect of different

materials based on overlapping images from different viewing angles. Using the proposed framework, we can measure the reflected light in different directions from a single point, an area within an arbitrary polygon, or along a polyline path. Allowing the measurements of the BRDF of an area instead of a single point (or footprint) will also improve the ability to understand the influence of the BRDF affect different scales and resolutions.

### 2. METHODOLOGY

The proposed methodology combines five main steps: a) multiview imaging and Structure From Motion (SFM) process for camera positioning, b) creating a connectivity graph and shortest path from base image to other images, c) sampling an ROI in the base image, and tracking the ROI in each image along the path, d) compute the mean reflectance for the ROI in the different images and e) modeling the BRDF of the ROI and correcting the reflectance.

#### 2.1 Multiview spectral and RGB imaging

We used the Specim IQ camera from Specim (Oulu, Finland, year of manufacture 2020). The camera is a handheld push broom system featuring integrated controls and an operating system. It combines two separate imaging sensors for hyperspectral and RGB data. The hyperspectral sensor provides images with  $512 \times 512$  pixels and 204 spectral bands between 400-1000 nm acquired by a push-broom line scanner with an internal rotating mechanism. The visible sensor provides RGB images with  $1280 \times 960$  pixels with an area of  $645 \times 645$  that overlaps with the image from the spectral sensor.

#### 2.2 Structure From Motion (SFM) for Camera Positioning

Given a set of acquiring images of the same object from different viewing directions, the SFM determines the camera location and orientation corresponding to each image (Jiang, 2020). The SFM

\* Corresponding author.

involves using various techniques such as point detection (Saleem, 2018), feature extraction, finding transformations between cameras, and calculating camera movements. We use the SFM to estimate the accurate camera location for each RGB image acquired in the multiview imaging step. RGB images are preferable instead of spectral ones for the SFM due to their higher spatial resolution and contrast.

### 2.3 Graph theory and Shortest-Path for Object Tracking

Graph theory describes the relationships between different objects or observations (Wang, 2015). The graph offers a flexible data representation and saves time and resources when "traveling" from one node to another. In this regard, the shortest-path strategy (Goldberg and Harrelson, 2005) is a fundamental problem in graph theory that consists of finding the path between two nodes in a directed graph with a minimal sum of the edges' weight along the path. Thus, we use graph theory to enable a dynamic transition between the acquired images (see

Figure 1). Accordingly, we can track an arbitrary ROI that we sample in one image and automatically determine its projection onto the other images in the set. For this purpose, we first find a set of tie points between each pair of images using the Speeded-up Robust Features (SURF) method (Oyallon and Rabin, 2015). Then, we use the detected tie points to estimate the geometrical transformation between the image pair. Besides, we use the number of detected tie points to calculate the weight of the arc that connects these two images in the connected graph as follows:

$$w_{i,j} = w_{j,i} = 1/p_{i,j} \quad (1)$$

where  $p_{i,j}$  and  $w_{i,j}$  are the number of tie points detected between images  $i$  and  $j$ , and the weight of the corresponding arc connecting between them in the graph, respectively. Accordingly, the detection of more points between a pair of images leads to a smaller weight (cost) of the arc connecting them, meaning it is "more profitable" to move along this arc while searching for the shortest path.

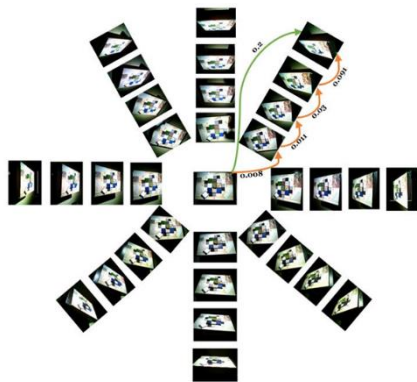


**Figure 1.** An illustration of multiview 33 images with an example of a direct path (green line) and the shortest path (indicated with orange lines) between two images.

We start by sampling a polygon, i.e., region of interest (ROI), representing the object/landcover we are interested in measuring its BRDF. In practice, we automatically sample the ROI in the nearly vertical image and detect its corresponding projection onto the other images, relying on the described shortest path strategy.

### 2.4 BRDF modeling and correction

As a final evaluation of the proposed methodology, we examined the performance of a common BRDF correction strategy on the obtained measurements. Accordingly, to minimize the negative influence of the BRDF effect on the spectral data, we correct the measured reflectance from the different directions to a reference direction (the nadir view). Such a correction calculates an anisotropy factor that describes the ratio between the measuring and reference directions. To calculate the anisotropy factor for each viewing direction, we first need to model the BRDF for each landcover type. Therefore, several models exist for describing and correcting BRDF effects on spectral images. Here we use the proposed model by Jia et al. (Jia et al., 2020). The model is based on a kernel-driven BRDF approach using a linear combination of three kernels: 1) A volumetric kernel represents the intrinsic property of the surface/object. It quantifies the reflected radiation from randomly distributed small facets (Kawata, 2008). A commonly used kernel is the hotspot-revised Ross-Thick-Maignan (RTM) kernel by Maignan et al. (Maignan et al., 2004). 2) A geometric kernel models the geometric structure of opaque reflectors and shadowing effects, as described in the Li-Transit-Reciprocal (LTR) kernel (Li et al., 1999). 3) A component of isotropic scattering is assumed to be uniform over the entire image for a given spectral band. Then, the BRDF model is described as follows:

$$\rho(\theta_i, \theta_r, \Delta\phi, c, \lambda) = f_{iso}(c, \lambda) + f_{vol}(c, \lambda)k_{vol}(\theta_i, \theta_r, \Delta\phi) + f_{geo}(c, \lambda)k_{geo}(\theta_i, \theta_r, \Delta\phi) \quad (2)$$

where  $\theta_i$  and  $\theta_r$  are the illumination and viewing zenith angles, respectively.  $\Delta\phi$  is the relative azimuth angle between the illumination source and the camera position,  $c$  indicates a material or landcover type, and  $\lambda$  corresponds to a particular spectral band.  $f_{iso}$ ,  $f_{vol}$  and  $f_{geo}$  are coefficients (weights) of isotropic, volumetric, and geometric scattering, respectively, and  $k_{vol}$  and  $k_{geo}$  are the volumetric and geometric scattering kernels, respectively.

After defining the general model, we estimate the kernel coefficients for each landcover type at each spectral band by solving a system of linear equations. Given  $n$  measurements of the same landcover type, but from different viewing directions, each measurement contributes a single equation as follows:

$$\begin{cases} f_{iso} + f_{vol}k_{vol}^1 + f_{geo}k_{geo}^1 = \rho_1 \\ f_{iso} + f_{vol}k_{vol}^2 + f_{geo}k_{geo}^2 = \rho_2 \\ \vdots \\ f_{iso} + f_{vol}k_{vol}^n + f_{geo}k_{geo}^n = \rho_n \end{cases} \quad (3)$$

which we can write in a matrix form as

$$\mathbf{Kf} = \mathbf{r}, \quad (4)$$

where,

$$\mathbf{K} = \begin{bmatrix} 1 & k_{vol}^1 & k_{geo}^1 \\ 1 & k_{vol}^2 & k_{geo}^2 \\ \vdots & \vdots & \vdots \\ 1 & k_{vol}^n & k_{geo}^n \end{bmatrix}, \mathbf{f} = \begin{bmatrix} f_{iso} \\ f_{vol} \\ f_{geo} \end{bmatrix}, \text{ and } \mathbf{r} = \begin{bmatrix} \rho_1 \\ \rho_2 \\ \vdots \\ \rho_n \end{bmatrix}. \quad (5)$$

The terms  $k_{vol}^1, k_{vol}^2, \dots, k_{vol}^n$  and  $k_{geo}^1, k_{geo}^2, \dots, k_{geo}^n$  represent the values of the volumetric and geometric scattering kernels corresponding to the 1st, 2nd, . . . ,  $n$ th observed reflectance measurements, i.e.,  $\rho_1, \rho_2, \dots, \rho_n$ , respectively. Accordingly, to correct the entire spectra for each landcover type, we defined a similar problem for each spectral band separately (Jia et al., 2020). Then, we achieve an estimation of coefficient vector, i.e.  $\hat{\mathbf{f}}$ , by solving an unconstrained least-squares problem as follows:

$$\hat{\mathbf{f}} = (\mathbf{K}^T \mathbf{K})^{-1} \mathbf{K}^T \mathbf{r} \quad (6)$$

Next, we calculate the vector of modeled reflectance  $\mathbf{r}_{in} = [\rho_{m,1}, \rho_{m,2}, \dots, \rho_{m,n}]^T$ , corresponding to the measured reflectance  $\mathbf{r} = [\rho_1, \rho_2, \dots, \rho_n]^T$  by

$$\mathbf{r}_{in} = \mathbf{K} \hat{\mathbf{f}}. \quad (7)$$

Finally, we compute the anisotropy factor (ANIF) for each measurement as given by:

$$ANIF = \frac{\rho_m \theta_i, \theta_r, \Delta\phi, c, \lambda}{\rho_m \theta_i, \theta_r = 0^\circ, \Delta\phi, c, \lambda}, \quad (8)$$

and calculate the corrected reflectance  $\rho_c$  as follows

$$\rho_c = \frac{\rho}{ANIF} \quad (9)$$

### 3. DATA ACQUISITION AND EXPERIMENTAL EVALUATION

#### 3.1 Hyperspectral and RGB Data of BRDF Scenes

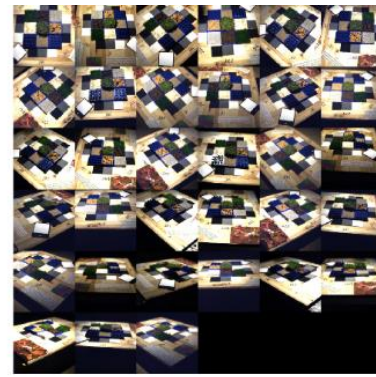
We chose nine materials to examine the BRDF measurement and correction for various landcover types (see Figure 2). We placed the light source at the position with an azimuth of 73 degrees and a zenith of 42.5 degrees relative to the normal of the tested scene. Besides, we placed a barium sulfate (BaSO<sub>4</sub>) calibration panel (Biggar et al., 1988) within the acquired frame in each image for efficient spectral calibration. We maintained a one-meter distance between the camera and the sample's plate center throughout the experiment. The RGB and spectral images were obtained simultaneously. First, we positioned the camera at the nadir and acquired the vertical image.

Next, we moved to zenith 30 degrees, placed the camera each time at a 45-degree interval from the previous azimuth, and acquired an image. Then, we continued until we reached the zenith of 70 degrees. Accordingly, our data set includes 33 spectral and corresponding RGB images, as Figure 3 shows. Finally, both the RGB and the spectral cameras were

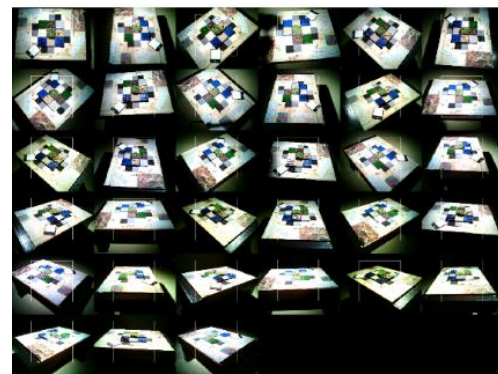
photogrammetric calibrated using a 2D pattern of the chessboard type with 29 mm square (Douskos et al., 2006).



**Figure 2.** The nine different materials used in experiment (a) were placed on top of a wooden plate marked with a circle of azimuths (b).



(a)



(b)

**Figure 3.** Set of 33 RGB images (a) and spectral images (b) from the vertical image through images of Zenith 30, 45, 60, to 70 degrees.

#### 3.2 Reflectance retrieval

We used the radiance images obtained by the camera to compute the average radiance and reflectance of the sampled ROI values in each acquired image as follows:

- 1) First, we averaged the radiance values of all pixels within the sampled ROI as follows

$$L_{material} \theta_i, \theta_r, \Delta\phi, \lambda = \frac{\sum_{i=1}^{i=np} L_{p_i} \theta_i, \theta_r, \Delta\phi, \lambda}{np} \quad (10)$$

where  $L_{p_i}$  is the recorded radiance value at the  $i$ th pixel, out of  $np$  pixels within the sampled ROI.

2) Then we calculate its reflectance as follows:

$$\rho_{material}(\theta_i, \theta_r, \Delta\phi, \lambda) = \frac{L_{material}(\theta_i, \theta_r, \Delta\phi, \lambda)}{L_{ref}(\theta_i, \theta_r, \Delta\phi, \lambda)} \quad (11)$$

where  $L_{ref}$  is the average radiance of the reference BaSO4 panel under the same specified conditions of illumination and viewing (zenith and azimuth angles).  $\theta_i, \theta_r, \Delta\phi$  and  $\lambda$  are the illumination zenith angle, view zenith angle, relative azimuth angle between the illumination source and the camera position, and the central spectral band wavelength.

### 3.3 Quantitative Evaluation of the BRDF measurement and Correction

To evaluate the results of measuring and correcting the BRDF, we observed the obtained reflectance values before and after the correction. We use the coefficient of variation (CV) statistics as a quantitative evaluation. Accordingly, we calculated the CV of the obtained reflectance of a specific landcover type from the different viewing angles. The CV in each spectral band is given by the ratio of the standard deviation  $\sigma_\lambda$  to the mean  $\mu_\lambda$  of the measurements as follows:

$$CV_\lambda = 100 \cdot \frac{\sigma_\lambda}{\mu_\lambda} \quad (12)$$

where  $\mu_\lambda = \frac{1}{n} \sum_{p=1}^n \rho_{p,\lambda}$  and  $\sigma_\lambda = \sqrt{\frac{1}{n} \sum_{p=1}^n \rho_{p,\lambda}^2 - \mu_\lambda^2}$  are the mean and standard deviation over the  $n$  measured pixels at the spectral band denoted by  $\lambda$ , respectively, and  $\rho_{p,\lambda}$  is the reflectance value at the  $p$ -th pixel. Then, for each landcover type, we computed the following statistical measures:

$$\overline{CV} = \frac{1}{n_\lambda} \sum_{\lambda=1}^{n_\lambda} CV_\lambda$$

$$\text{std } CV = \sqrt{\frac{\sum_{\lambda=1}^{n_\lambda} CV_\lambda^2 - \overline{CV}^2}{n_\lambda}} \quad (13)$$

$$\max CV = \max CV_\lambda, \text{ for } \lambda = 1, 2, \dots, n_\lambda$$

where,  $\overline{CV}$ ,  $\text{std } CV$ , and  $\max CV$  are the mean, standard deviation, and maximal value of the CV, respectively, and  $n_\lambda$  is the number of spectral bands.

### 3.4 Experimental Testing

We first built the connectivity between all RGB images and calculated initial relative locations for each camera (location and orientation) as initial values for the Bundle Adjustment phase. Then we used the SFM process to estimate the correct camera

locations and create a 3D model of the scene. In addition to examining our code in MATLAB for SFM, we used Meshroom and cloudCompare software. Finally, we calculated the camera locations in the local system by computing the zenith angle and azimuth for each camera position. Figure 4 presents the locations in a top view of the local polar system.

Here we focused on the measurements on the main profiles to evaluate our methodology's performance (see Figure 4). In particular, we selected the principal plane, which contains the object, the light source, spectral sensor. In our case, the principal plane profile includes the images in azimuth 90 to 270 degrees.

To validate our methodology, we applied the following steps to the different types of materials on the two profiles:

- Sample an ROI in the base (vertical) image.
- Compute the shortest path from the base image to each other image.
- Track the ROI in each image along the path.
- Compute the mean reflectance for the ROI in the different images.
- Model the BRDF of the ROI, compute the anisotropy factor and correct the reflectance.

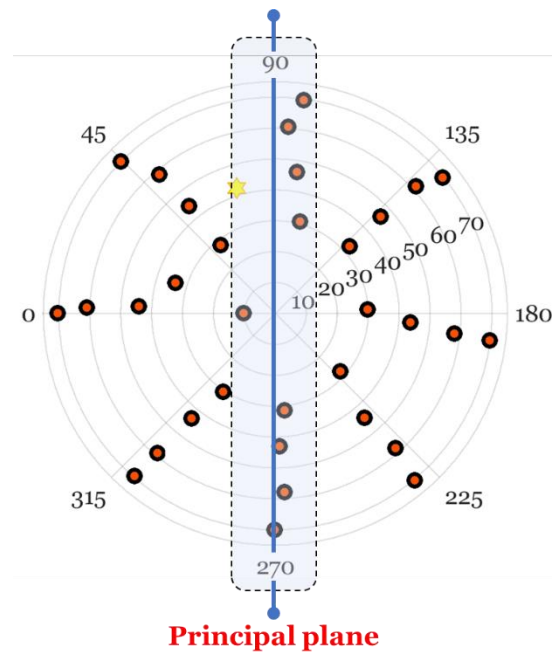


**Figure 4.** A top view of all estimated camera locations as obtained through SFM. The numbers 0 to 315 on the circumferential circle and 10 to 70 between the various circles indicate azimuth and zenith angles in degrees, respectively. We consider the locations within the rectangular area as approximately placed within the principal plane.

## 4. RESULTS AND DISCUSSION

To study the BRDF of a given land cover type, we observed and modeled the measurements and corrected reflectance values at the nine zenith angles on the selected profile within the principal plane. First, we applied the proposed strategy for automatically tracking the sampled ROI. For example, Figure 5 presents the sampled ROI for Grass in the near-vertical image and automatically derived corresponding ROIs on the other images. Then, as mentioned before, the mean reflectance spectra in the

different viewing directions were extracted by averaging the ROIs in each spectral band.

Figure 6 illustrates the results for a selected wavelength. The corrected reflectance values are scattered around those obtained from the vertical image, i.e., the reference viewing direction. Such a scattering indicates a high accuracy correction of the BRDF. In addition, the light source is located at an azimuth of 73 degrees and a zenith of 42.5 degrees. The results show a "hot-spot" with maximal reflectance around this direction. This result agrees with the theoretical back-scattering effect and indicates the wellness of the BRDF measurements. Similarly, there is a decrease in the reflectance values due to the forward scattering at the other side of the selected profile on the principal plane (i.e., measurements from locations with an azimuth of 270 degrees).

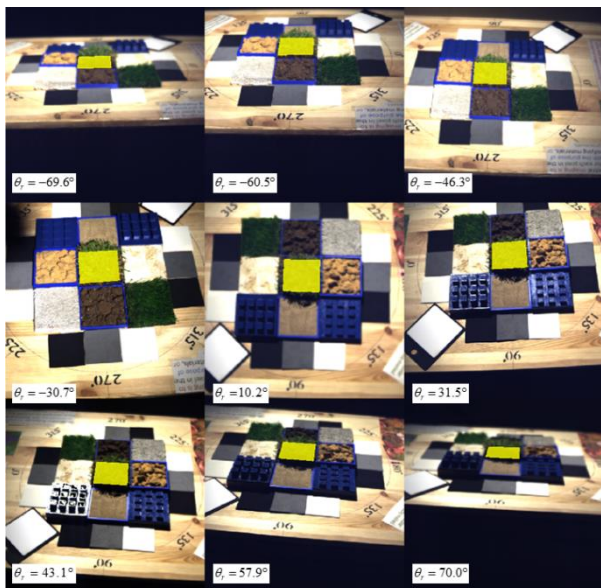


**Figure 5.** An example of a sampled ROI on the near-vertical image ( $\theta = 10.2^\circ$ ) for the landcover type Grass, and the corresponding ROIs on the other images on the profile of 90 to 270 degrees, as obtained by the proposed automatic tracking strategy.

Besides, Figure 7 presents the measured and corrected reflectance of the grass landcover and the corresponding CV values. The obtained spectral signatures of Grass have typical properties of vegetation spectra; high absorption in the red, high in the blue, and ultraviolet, whereas they have a peak of the reflectance in the green wavelength and high reflectance in the near-infrared (Division, 1989).

Moreover, the results clearly show the accuracy of the BRDF correction. The correction of data in 60 and 70 degrees is noticeable. Despite the inaccuracy in the measured reflectance in these two angles, the corrected reflectance values are closer to a vegetation signature. In general, the signatures for the different wavelengths are close to each other after the correction of the BRDF. Specifically, the reflectance values for wavelengths 650 to 750 nm are very close, and the CV of the corrected measurements in this region is accordingly low.

Along with the accuracy of the ROI tracking process, the BRDF correction has yielded good results. For example, the results for the light-soil landcover, presented in Figure 8, show a significant reduction in the CV of the corrected measurements. As a result, the variability between the reflectance values is much lower, and the signatures obtained from the different viewing angles are similar. To better understand the obtained results through

quantitative analysis, we examined the CV and its statistics of four materials in the scene. Table 1 summarizes the results.

Table 1 shows the noticeable differences in CV values before and after BRDF correction in landcover types. All the selected landcover types, i.e., natural Grass, synthetic Grass, brown soil, and light soil, are characterized by a relatively rough surface. However, the results reveal interesting outcomes. On the one hand, the obtained results for natural and synthetic Grass are highly similar. This outcome is correlated with the fact that these land covers have similar brightness and subpixel topographic structures. However, on the other hand, the brown and light soil land covers also have similar subpixel topography, but the obtained CV metrics for the measured reflectance are highly different. We believe that this difference happens due to the brightness difference. The variability of the brightness between illuminated and shaded facets in the light soil is more significant than in the brown soil. Thus, the CV of the light soil measurements is accordingly higher. However, the obtained CV for these two land covers after the BRDF correction is highly similar. Reducing the CV values indicates the importance of correcting the BRDF effect. Besides, it tells the proposed methodology's efficiency in accurately tracking ROIs and accordingly measuring the BRDF of different land cover types. Accordingly, it supports the conclusion that we accurately measure the BRDF through the images.

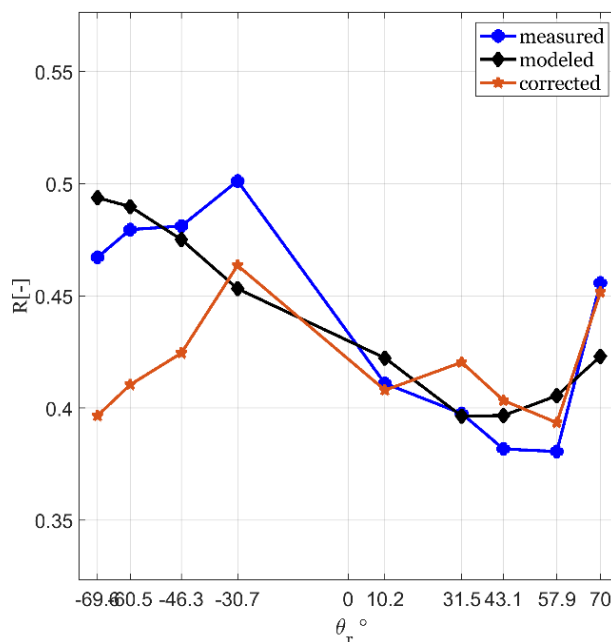


**Figure 6.** The measured, modeled, and corrected reflectance values at different zenith angles for profile 90-270 degrees at wavelength 513.4 nm.

Material	$\overline{CV}$		$\max(CV)$		$std(CV)$	
	$\rho$	$\rho'$	$\rho$	$\rho'$	$\rho$	$\rho'$
Grass	12.37	5.84	14.59	7.42	2.21	1.1
Synthetic Grass	13.53	5.52	16.81	6.45	2.41	0.68
Light Soil	23.31	5.21	27.52	6.44	3.93	0.97
Brown Soil	6.74	5.93	7.9	7.32	0.81	0.85

**Table 1**

Statistic of CV parameters for different materials.  $\rho$  and  $\rho'$  are the measured and corrected reflectance measurements, respectively.

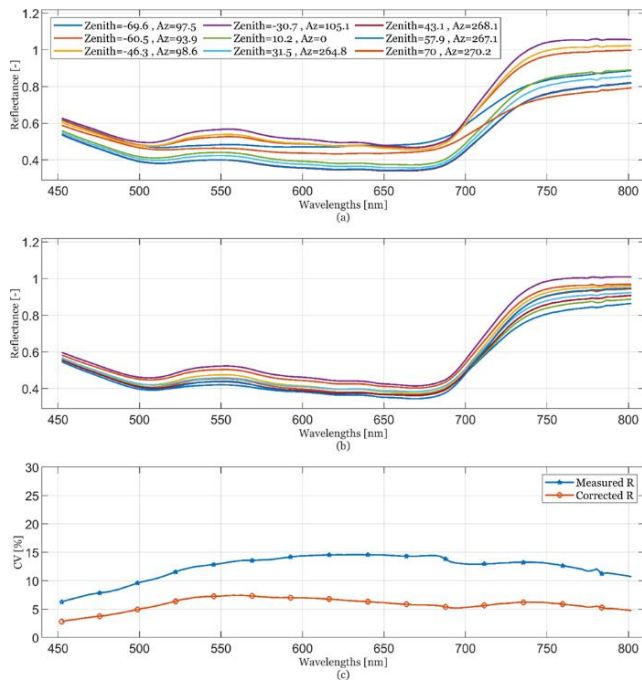


**Figure 7.** The reflectance values of the Grass ROI before correction (a), after correction (b), and the statistics CV of reflectance values at different zenith angles (c).

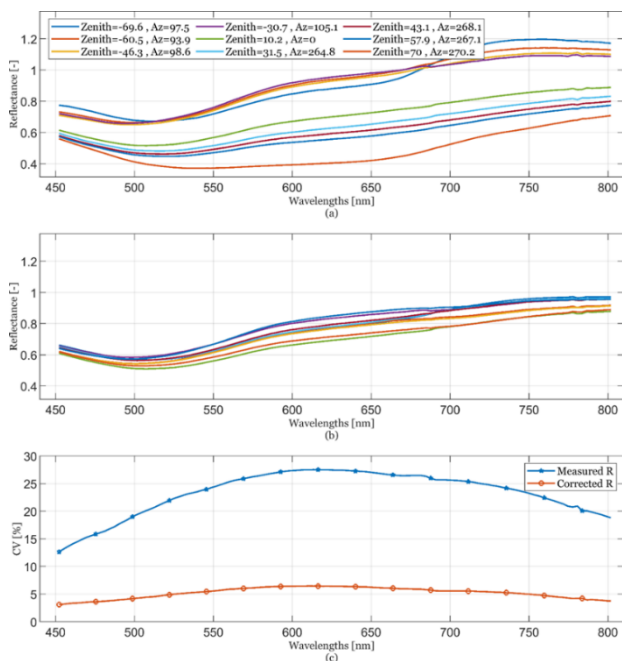


**Figure 8.** The reflectance values of the Light Soil ROI before correction (a), after correction (b), and the statistics CV of reflectance values at different zenith angles (c).

## 5. CONCLUSION

This article presented a new study regarding the BRDF measurement and proposed a new methodological framework. This framework contributes to studying the BRDF of different materials and landcover types by automatically measuring surface directional reflectance. It reduces the complexity of such measurements and the analysis of the BRDF by allowing

automatic 3D positioning of the acquired images without using special and expensive instruments, analyzing the BRDF of different shapes, and accessible analysis of objects' BRDF in different scales and resolutions. Moreover, our methodology can also be applied to drone-based imaging. In this regard, existing studies addressing the image-based BRDF (Hakala et al., 2018) usually use one or very few images relying on the assumption that similar landcover types can appear in different pixels accordingly being measured from different directions. In contrast, the proposed methodology is suitable for datasets with many overlapping images. Thus, it allows for analyzing the BRDF of a given land cover type's same point/ROI from a broader range of directions.

To evaluate the proposed methodology's performance and test the impact of the BRDF, we experimented with data acquired under controlled conditions. In the case of materials with smooth surfaces, the results revealed that the effect of the BRDF is uniform. In contrast, the effect is neither uniform nor has a specific intensity in rough materials. The results clearly showed that our strategy for tracking and optimizing the ROI's location in different images is accurate. Moreover, using the kernel-driven BRDF approach for correcting the BRDF effects obtained accurate results in reducing the CV of spectral signatures for the examined materials.

## REFERENCES

- Biggar, S.F., Labeled, J., Santer, R.P., Slater, P.N., Jackson, R.D., Moran, M.S., 1988. Laboratory Calibration Of Field Reflectance Panels. *Recent Adv. Sensors, Radiom. Data Process. Remote Sens.* 0924, 232. <https://doi.org/10.1117/12.945691>
- Division, E., 1989. Spectral reflectance characteristics of vegetation and their use in estimating productive potential 99, 59–81.
- Douskos, V., Kalisperakis, I., Karras, G., 2006. Automatic Calibration of Digital Cameras Using Planar Chess-Board Patterns. *Camera*.
- Foo, S.C., 1997. A GONIOREFLECTOMETER FOR MEASURING THE BIDIRECTIONAL REFLECTANCE OF MATERIAL FOR USE IN ILLUMINATION COMPUTATION.
- Goldberg, A. V., Harrelson, C., 2005. Computing the shortest path: A\* search meets graph theory. *Proc. Annu. ACM-SIAM Symp. Discret. Algorithms* 156–165.
- Hakala, T., Markelin, L., Id, E.H., Scott, B., Theocharous, T., Id, O.N., Näsi, R., Suomalainen, J., Id, N.V., Greenwell, C., 2018. Direct Reflectance Measurements from Drones : Sensor Absolute Radiometric Calibration and System Tests for Forest Reflectance Characterization. <https://doi.org/10.3390/s18051417>
- Jia, W., Pang, Y., Tortini, R., Schläpfer, D., Li, Z., Roujean, J.L., 2020. A kernel-driven BRDF approach to correct airborne hyperspectral imagery over forested areas with rugged topography. *Remote Sens.* 12. <https://doi.org/10.3390/rs12030432>
- Jiang, S., 2020. Efficient structure from motion for large-scale UAV images : A review and a comparison of SfM tools. *ISPRS J. Photogramm. Remote Sens.* 167, 230–251. <https://doi.org/10.1016/j.isprs.2020.04.016>
- Kawata, Y., 2008. Introduction of the shadowing kernel for brdf analysis, in: *International Geoscience and Remote Sensing Symposium (IGARSS)*. Institute of Electrical and Electronics Engineers Inc., pp. 793–796. <https://doi.org/10.1109/IGARSS.2008.4779468>
- Li, X., Gao, F., Chen, L., Strahler, A.H., 1999. Derivation and

validation of a new kernel for kernel-driven BRDF models. *Remote Sens. Earth Sci. Ocean. Sea Ice Appl.* 3868, 368. <https://doi.org/10.1117/12.373123>

Maignan, F., Bréon, F.M., Lacaze, R., 2004. Bidirectional reflectance of Earth targets: Evaluation of analytical models using a large set of spaceborne measurements with emphasis on the Hot Spot. *Remote Sens. Environ.* 90, 210–220. <https://doi.org/10.1016/j.rse.2003.12.006>

Nicodemus, F., Richmond, J., Hsia, J., 1977. Geometrical considerations and nomenclature for reflectance. *Sci. Technol.* 60, 1–52. <https://doi.org/10.1109/LPT.2009.2020494>

Oyallon, E., Rabin, J., 2015. An Analysis of the SURF Method. *Image Process. Line* 5, 176–218. <https://doi.org/10.5201/ipol.2015.69>

Riviere, N., Ceolato, R., Hespel, L., 2012. Multispectral polarized BRDF: Design of a highly resolved reflectometer and development of a data inversion method. *Opt. Appl.* 42, 7–22. <https://doi.org/10.5277/oa120101>

Román, M.O., Gatebe, C.K., Schaaf, C.B., Poudyal, R., Wang, Z., King, M.D., 2011. Remote Sensing of Environment Variability in surface BRDF at different spatial scales ( 30 m – 500 m ) over a mixed agricultural landscape as retrieved from airborne and satellite spectral measurements. *Remote Sens. Environ.* 115, 2184–2203. <https://doi.org/10.1016/j.rse.2011.04.012>

Saleem, Z., 2018. A Comparative Analysis of SIFT , SURF , KAZE , AKAZE , ORB , and BRISK. 2018 Int. Conf. Comput. Math. Eng. Technol. 1–10. <https://doi.org/10.1109/ICOMET.2018.8346440>

Schaepman-strub, G., Schaepman, M.E., Painter, T.H., Dangel, S., Martonchik, J. V, 2006. Reflectance quantities in optical remote sensing — definitions and case studies 103, 27–42. <https://doi.org/10.1016/j.rse.2006.03.002>

Shen, H., Abuduwaili, J., Ma, L., Samat, A., 2019. Remote sensing - based land surface change identification and prediction in the Aral Sea bed , Central Asia 2031–2046. <https://doi.org/10.1007/s13762-018-1801-0>

Wang, X., 2015. Graph based approaches for image segmentation and object tracking To cite this version. *Ec. Cent. Lyon.*